Cosmic-ray isotope measurements with HELIX

P. Allison[1], J. J. Beatty[1], L. Beaufore[2], Y. Chen[3], S. Coutu[3], E. Ellingwood[4], M. Gebhard[5], N. Green[6], D. Hanna[4], B. Kunkler[5], I. Mognet[3], R. Mbarek[2], K. McBride[1], K. Michaels[5], D. Müller[2], J. Musser[5], S. Nutter[7], S. O'Brien[4], N. Park[*†8], T. Rosin[4], E. Schreyer[2], G. Tarlé[6], M. Tabata[9], A. Tomasch[6], G. Visser[5], S. P. Wakely[2], T. Werner[2], I. Wisher[2], and M. Yu[3]

[1]*The Ohio State University, Columbus, OH 43210 USA*

[2]*University of Chicago, Chicago, IL 60637 USA*

[3]*Pennsylvania State University, University Park, PA 16802 USA*

[4]*McGill University, Montreal, QC H3A 2T8, Canada*

[5]*Indiana University, Bloomington, IN 47405 USA*

[6]*University of Michigan, Ann Arbor, MI 48109 USA*

[7]*Northern Kentucky University, Highland Heights, KY 41099 USA*

[8]*University of Wisconsin-Madison, Madison, WI 53706 USA*

[9]*Chiba University, Chiba, 263-8522, Japan*

HELIX (High Energy Light Isotope eXperiment) is a balloon-borne experiment designed to measure the chemical and isotopic abundances of light cosmic ray nuclei. Detailed measurements by HELIX, especially of ^{10}Be from 0.2 GeV/n to beyond 3 GeV/n, will provide an essential set of data for the study of propagation processes of the cosmic rays. HELIX consists of a 1 Tesla superconducting magnet with a high-resolution gas tracking system, time-of-flight detector, and a ring-imaging Cherenkov detector. The instrument is scheduled to have a long-duration balloon flight out of McMurdo Station during NASA's 2020/21 Antarctic balloon campaign. Here, we discuss the scientific goals and the design of the experiment, and report on its current status.

---

*Speaker.

†E-mail:npark7@wisc.edu

1. Introduction

Since the discovery of the cosmic rays in 1912, understanding the origin, acceleration mechanisms, and propagation of these high-energy particles has been an important scientific goal. While our knowledge of cosmic rays has been improved significantly over the last hundred years, definite answers to these questions are still elusive. Understanding the propagation of cosmic rays has become more important recently as the space-borne detectors, such as PAMELA and AMS-02, started to reveal new features in the cosmic-ray spectra. One of the most striking results has been the discovery of an excess of positrons above 25 GeV that was not expected from simple propagation models [1, 2]. The new measurements also show that the proton and helium spectra deviate from an expected single power-law distribution at a rigidity of around 300 GV, with the spectral indexes becoming harder for higher energies [3, 4, 5]. This spectral hardening has been observed for the fluxes of other elements up to oxygen as well. There have been several models to explain these new features by adding new astrophysical sources of particles, considering the contributions from different sources, adding contributions from exotic particles, and considering different propagation effects. A better understanding of the propagation of high energy particles in our Galaxy would provide key information to distinguish one scenario from the other.

The data most commonly used to study the propagation of cosmic rays are measurements of the boron-to-carbon ratio, where boron is a secondary nucleus generated by the inelastic scattering of primary nuclei with the medium and carbon is a primary nucleus originating from the source. This ratio probes the total material path length traversed by the cosmic rays during their containment time in our Galaxy before they reach the Earth. It thus has a degeneracy between the material density and the containment time of the cosmic rays. Measurements of radioactive isotopes with known decay times can provide a direct measurement of the containment time of the cosmic rays, removing some of the degeneracy. Among the radioactive isotopes, there are a few, referred to as "propagation clock" isotopes, that have a half-life closed to the containment time of the cosmic rays. The isotope beryllium-10 (^{10}Be), with a β–decay half-life of 1.39 Myr, is the best measured among these propagation clock isotopes, with measurements up to $\sim$2 GeV/n by the ISOMAX experiment [6]. However, the statistical errors on the measurements are relatively large due to the short exposure of the experiment.

The High Energy Light Isotope eXperiment (HELIX) is a new long-duration balloon payload designed to measure light isotopes from 0.2 GeV/n eventually up to $\sim$10 GeV/n. HELIX can measure isotopes from proton (Z=1) up to neon (Z=10), and the detector is optimized to provide precision measurements of the ratio of the beryllium isotopes—the ratio between radioactive ^{10}Be to stable ^{9}Be. High-quality ^{10}Be/^{9}Be measurements can provide strong discrimination (especially at energies of $\sim$3 GeV/n) between entire classes of propagation models [6, 7, 8].

2. HELIX Instruments

HELIX is a magnet spectrometer designed for a long-duration balloon flight. The instrument is designed to measure the light cosmic-ray isotopes with good precision, especially for the isotopes of beryllium. The full configuration of the detector is shown in Figure 1. Tracking information from the drift chamber tracker (DCT) inside a strong magnetic field provided by a superconducting
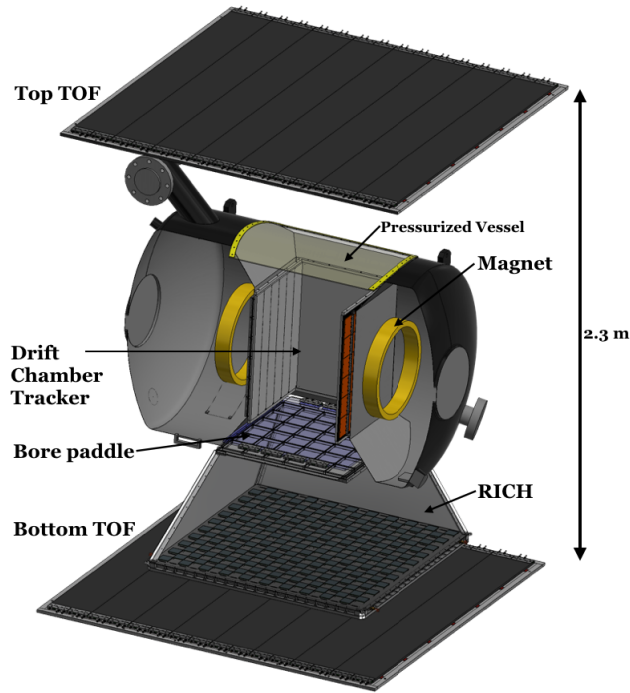
Figure 1: Partially sectioned 3D model of the HELIX detector systems, showing the superconducting magnet, drift chamber tracker, top and bottom time-of-flight layers, bore paddle, and ring-imaging Cherenkov detector.

magnet provides a rigidity measurement of the incident particles. With a 1 T magnetic field and good spatial resolution provided by the DCT, HELIX has a rigidity resolution of better than 2.5% for ^{10}Be measurements up to $\sim$3 GeV/n. The velocity of incident particles will be measured with two different detectors–a time-of-flight (TOF) detector with scintillator paddles for the particles with energies up to $\sim$1 GeV, and a ring-imaging Cherenkov (RICH) detector for the particles with energies higher than 1 GeV. Combining the TOF and RICH measurements, HELIX achieves a velocity resolution of $\Delta\beta/\beta \sim 1 \times 10^{-3}$ from 0.1 GeV/n up to $\sim$3 GeV/n for beryllium isotopes. Combining the rigidity and velocity information, the expected mass resolution for HELIX is $\sim$3% for ^{10}Be/^{9}Be measurements up to $\sim$3 GeV/n.

One of the challenges for HELIX is to operate the detector within a strong magnetic field. For efficient measurement of signals within this field, HELIX utilizes the most recent generation of silicon photomultiplier (SiPM) technology instead of the traditional photomultiplier tubes (PMTs) for the TOF and RICH. SiPMs require a lower bias voltage (30 V) compared to PMTs (a few kV), which is an additional advantage because a low-voltage power supply does not require any special design to avoid the corona problem frequently encountered with high-voltage power supplies. The thermal noise of SiPMs is much higher than that of PMTs and their performance has a strong correlation with the temperature of the device. For stable operation, we have carefully designed the thermal environment for the detector including a compensation system based on ambient temperature monitoring. Also, due to the strong magnetic field, omni-directional solar panel arrays were chosen rather than relying on a rotator to point the solar panels toward the Sun.

We have built prototype detectors for testing for the final designs, and now are constructing
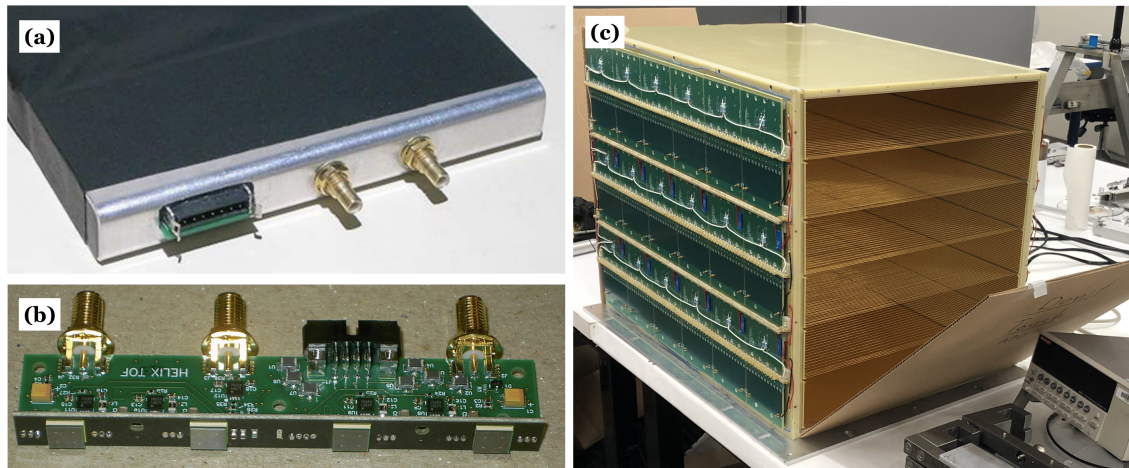
Figure 2: (a) One end of the prototype TOF paddle mounted with a prototype SiPM carrier board. (b) The final TOF front-end electronics board assembled with a SiPM carrier board. (c) Fully strung DCT.

flight hardware, with a goal to integrate systems in fall of 2019. We are scheduled to have an integration test in 2019. A brief description of the main detector components as well as the status of each is presented in the following sections.

2.1 Superconducting Magnet

The superconducting magnet located at the center of HELIX can provide an approximately uniform 1 T magnetic field within a rectangular warm bore. The magnet was initially designed and built by Cryomagnetics for the HEAT experiment. It contains two superconducting coils immersed in a liquid-helium (LHe) bath to keep the coil temperature lower than the critical temperature of 9.8 K. The cryostat can contain 260 liters of LHe, providing a hold time of approximately 7 days. The magnet has been used in five successful balloon campaigns, where it was operated within a pressure vessel. Cryomagnetics refurbished the magnet for HELIX to make it functional in vacuum. The refurbished magnet was successfully tested for vacuum operations at the Large Vacuum Test Facility at the University of Michigan in 2019. The magnetic field in the bore volume has been mapped in three dimensions, and the measurements match well with values from a theoretical model.

2.2 Time-of-Flight and Charge System

The HELIX TOF and charge system consists of three layers of 1 cm thick scintillator paddles. Two main layers are located at the top and bottom of the detector frame, with a separation of 2.3 m. Each top and bottom TOF layer has 8 scintillator paddles with 20 cm width and 1.6 m length, providing a total active area of 2.56 m^2 per layer. Each paddle is read out by 16 SiPMs: eight SiPMs at each end. The flight-ready front-end electronics board with a SiPM carrier board and one end of a prototype paddle equipped with a prototype SiPM carrier board are shown in Figure 2. With a 10 psec TDC system, the TOF system provides a timing resolution of <50 psec for Z>3 nuclei, which will be sufficient to measure the velocity of these particles up to 1 GeV/n with good precision. There is a smaller scintillator layer located between the DCT and the radiator of the
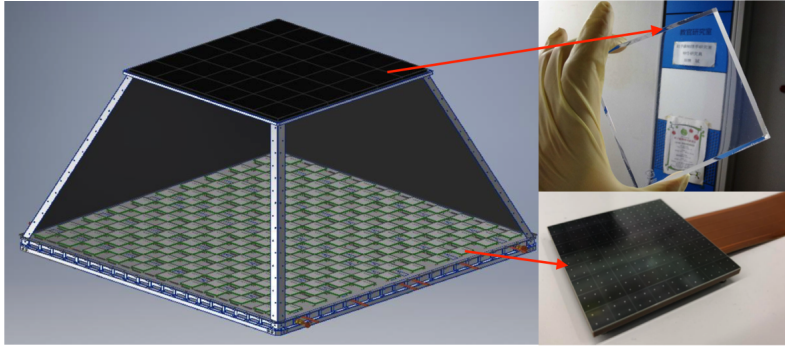
Figure 3: 3D model of RICH designed for HELIX with side panels opened to show the checkerboard pattern of the focal plane. An aerogel tile is shown on the upper right side, and a 64-channel Hamamatsu SiPM array with flexible PCB cable is shown on the lower right side of the figure.

RICH, referred to as the "bore paddle." Consisting of a single scintillator plate with dimensions of 0.6 m by 0.6 m, this paddle constrains the trigger geometry to particles passing through the center of the detector, thus reducing the overall trigger rate. The bore paddle is read out by 32 SiPMs: 16 SiPMs along each of two opposite edges. The combination of the top and bottom layers with the bore paddle layer provides the system-wide trigger. The three layers measure the charge of incident particles up to Z=10.

2.3 Drift Chamber Tracker

The gas-filled multi-wire drift chamber tracker is located inside the bore of the magnet to measure the trajectory of incident particles. A gas detector is preferred to minimize Coulomb scattering, which dominates rigidity resolution at low energy. The DCT consists of 72 layers with each layer containing three drift cells, and fills a volume of 45cm by 45cm by 58cm. With a low diffusion drift gas, such as CO_2, a drift field of 1 kV/cm, and high-speed sampling readout electronics, the DCT is designed to achieve a mean spatial resolution of 65 μm for Z>3 particles. The DCT is placed inside a pressurized vessel that fits in the bore of the magnet. The pressurized vessel is designed to maintain 1 atm pressure during the flight. The vessel was installed within the bore of the magnet during a magnet vacuum operation test in 2019, and held the 1 atm pressure in flight-like vacuum conditions. The wires have been fully installed in the DCT as shown in the right panel of Figure 2, and the final stages of high voltage testing with front-end electronic board installation are under way.

2.4 Ring Imaging Cherenkov Detector

The proximity-focused aerogel RICH designed for HELIX provides velocity measurements of particles with energies higher than 1 GeV/n. The radiator of the RICH consists of 36 square aerogel tiles with 10 cm width and 1 cm thickness. Aerogel tiles with high transparency and high refractive index of 1.15 have been procured for HELIX by utilizing pin-drying technology [9]. The expansion length between the radiator and the focal plane is 50 cm. The focal plane has an area of ~1 m^2, and consists of an array of 64-channel Hamamatsu SiPM arrays with a pixel size of 36 mm^2. The focal plane is partially populated with sensors arranged in a checkerboard pattern. Figure 3 shows

the RICH mechanical model as well as an aerogel tile and the 64-channel SiPM array. The RICH is designed to achieve a β resolution better than 0.1%, which requires measurements of single photoelectron (p.e.) signals from the SiPMs and accurate knowledge of the refractive index of the aerogel radiator. To reduce the single p.e. rates from the dark current of the SiPMs, the focal plane is designed with a dedicated thermal layer to provide a stable and cool temperature. The details of the aerogel radiator procurement [10], refractive index measurements of the aerogel radiator [11], and overall RICH design and testing [12] can be found in the other HELIX contributions to this conference.

3. Data Acquisition

The data acquisition (DAQ) system of HELIX is based on a custom hierarchical architecture. Data from each subsystem is buffered by subsystem merger boards powered by Xilinx Artix-7 FP-GAs. Collected data in the subsystem merger board gets transferred to the master merger board by using the Aurora serial protocol over 10G SFP+ cables. The same interface is used for system monitoring and configuration. A mini-ITX science flight computer running Linux reads out the master merger over PCIE interface, stores data to SSD, and manages all telemetry and housekeeping operations. The DAQ system is triggered by the master trigger board, which generates two types of triggers, Z-LOW and Z-HI, based on the signal from the TOF. A lower threshold is set for the Z-LOW trigger for collecting mainly proton and helium data, and the Z-HI trigger is set to trigger on heavier nuclei. Both triggers can be set to pre-scale.

4. Power

The HELIX solar power system will use an omni-directional photovoltaic (PV) array with 4 sides with an angle of inclination of $\sim 22°$. Because of the high field of the magnet, the overall instrument at float will stray oriented to the local geomagnetic field. The omni-direction design is required to ensure that the payload will always have light incident on some panels. Each side of the solar array will have eight 31" $\times$ 27" PV panels, provided by Suncat, which provide enough power to run the instrumentation. Additional charging power will come from the non solar-facing panels that, due to the angle of incidence, will still receive enough light to generate an additional ~ 150 W. The multiple non-uniformly illuminated panels require independent maximum power point trackers to be used for each side, and ideal diode controllers to be used to control the combined power to minimize losses. This design has the benefit that it provides high reliability but still makes use of the redundant sides to generate extra power. Currently the PV panels have been delivered and the solar array is being constructed with operating tests planned for late summer of 2019.

5. Expected Performance

Figure 4 shows the expected performance of HELIX for ^{10}Be nuclei measurements. The plot on the left side shows the relative mass resolution of HELIX for ^{10}Be nuclei based on Monte Carlo simulations with the instrument configuration described above. As shown in the plot, HELIX can provide $\sim 3\%$ relative mass resolution for ^{10}Be nuclei from a few hundred MeV/n all the way to ~ 3
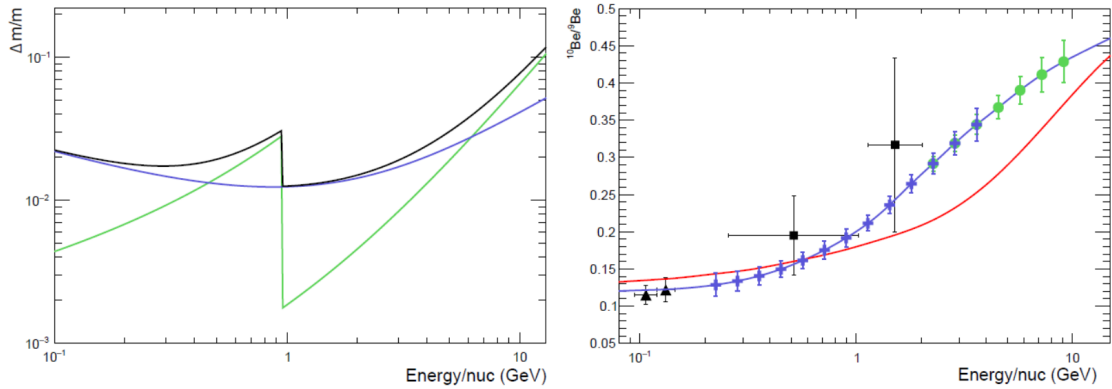
Figure 4: Left: Predicted relative mass resolution vs. energy per nucleon for the HELIX instrument with ^{10}Be incident particles. The blue line is the relative uncertainty on the mass measurement from the spectrometer; the green line is the γ^2-weighted contribution from the velocity-determining instrument: the TOF below 1 GeV/n and the RICH above 1 GeV/n. The black line is the sum in quadrature of the two. Right: Anticipated beryllium isotope ratio measured by HELIX. The blue crosses show results of 14-day exposure with the instrument configuration described here. The green dots show expected results for 28-day exposure with an upgraded instrument. The blue line represents a Leaky Box model with a low-density Local Bubble and the red line represents a diffusion halo model with re-acceleration [6]. Also shown on the plot are the results of ACE/CRIS (triangles) and ISOMAX (squares).

GeV/n, which corresponds to 0.3 a.m.u. separation between ^{9}Be nuclei and ^{10}Be nuclei. With 14 days of exposure, HELIX will provide data that can be compared with ACE/CRIS measurements in the low energies and well beyond the low-statistics measurement by ISOMAX at 1.1–2.0 GeV/n as shown in the right panel of Figure 4. In addition to the results from the exposure of 14 days with the instrument configuration described here, the expected results from a future 28-day exposure in an upgraded configuration are also shown in the figure. The upgraded configuration considered in the plot has better tracking resolution provided by silicon strip sensors with a longer magnet hold time provided by an updated cryostat system. Clearly, even the initial HELIX results will provide very strong constraints on the behavior of the ^{10}Be/^{9}Be ratio, reaching with good statistics well into the region where time dilation significantly affects the radioactive isotope lifetime. More than 1500 ^{10}Be nuclei are expected above 2 GeV/n with 14 days of exposure, a region where no measurements currently exist.

6. Future Plan

Currently all of the sub detectors are under construction, scheduled to start the overall integration test in 2019 at the University of Chicago. Meanwhile the integration test of the data acquisition system has started along with flight software development. After environment and ground tests in early 2020, we are planning to have a long-duration balloon flight out of McMurdo Station during NASA's 2020/21 Antarctic balloon campaign.

References

[1] O. Adriani et al., Nature 458, 607 (2009)

[2] M. Aguilar et al., Phys. Rev. Lett. 110, 141102 (2013)

[3] O. Adriani et al., Science, 332, 6025, 69 (2011)

[4] M. Aguilar et al., Phys. Rev. Lett. 114, 171103 (2015)

[5] M. Aguilar et al., Phys. Rev. Lett. 115, 211101 (2015)

[6] T. Hams et al., ApJ 611, 892 (2004)

[7] M. Simon, 27th ICRC proceeding (1999)

[8] A. Putze et al., A&A 516, A66 (2010)

[9] M. Tabata et al., Nucl. Instrum. Meth. A (2019)

[10] M. Tabata et al., ICRC (2019)

[11] T. Rosin et al., ICRC (2019)

[12] I. Wisher et al., ICRC (2019)